

Surface potential microscopy of surfactant-controlled single gold nanoparticle

Hyungbeen Lee^{1,7} , Yoochan Hong^{2,3,7}, Dongtak Lee^{4,7} ,
Seungyeon Hwang², Gyudo Lee⁵ , Jaemoon Yang^{2,6,8}  and
Dae Sung Yoon^{4,8} 

¹ Center for BioMicrosystems, Korea Institute of Science and Technology, Seoul 02792, Republic of Korea

² Department of Radiology, College of Medicine, Yonsei University, Seoul 03722, Republic of Korea

³ Department of Medical Device, Korea Institute of Machinery and Materials (KIMM), Daegu Research Center for Medical Devices and Green Energy, Daegu 42994, Republic of Korea

⁴ School of Biomedical Engineering, Korea University, Seoul 02841, Republic of Korea

⁵ Department of Biotechnology and Bioinformatics, Korea University, Sejong 30019, Republic of Korea

⁶ Systems Molecular Radiology at Yonsei, Seoul 03722, Republic of Korea

E-mail: 177hum@yuhs.ac (J. Y.) and dsyoon@korea.ac.kr (D.S.Y.)

Received 29 October 2019, revised 7 January 2020

Accepted for publication 6 February 2020

Published 9 March 2020



CrossMark

Abstract

The surface potential of nanoparticles plays a key role in numerous applications, such as drug delivery and cellular uptake. The estimation of the surface potential of nanoparticles as drug carriers or contrast agents is important for the design of nanoparticle-based biomedical platforms. Herein, we report the direct measurement of the surface potential of individual gold nanorods (GNRs) via Kelvin probe force microscopy (KPFM) at the nanoscale. GNRs were capped by a surfactant, cetyltrimethylammonium bromide (CTAB), which was removed by centrifugation. CTAB removal is essential for GNR-based biomedical applications because of the cytotoxicity of CTAB. Applying KPFM analysis, we found that the mean surface potential of the GNRs became more negative as the CTAB was removed from the GNR. The results indicate that the negative charge of GNRs is covered by the electrostatic charge of the CTAB molecules. Similar trends were observed in experiments with gold nanospheres (GNS) capped by citrates. Overall, KPFM-based techniques characterize the surfactant of individual nanoparticles (i.e. GNR or GNS) with high resolution by mapping the surface potential of a single nanoparticle, which aids in designing engineered nanoparticles for biomedical applications.

Keywords: gold nanorod, gold nanosphere, capping agent, surface potential, Kelvin probe force microscopy

(Some figures may appear in colour only in the online journal)

Introduction

Functionalized gold nanoparticles (GNPs) have been widely utilized in a variety of biomedical applications including target delivery, biodetection, bioimaging, and antisense technology [1, 2]. Before functionalizing the GNPs, their stability is maintained by capping agents (i.e. surfactants), such as cetyltrimethylammonium bromide (CTAB) and

citrate. Functionalization of the GNPs can be achieved by replacing the surfactants with biomolecules, such as nucleic acids, enzymes, receptors, antibodies, and antigens, which provide steric and/or electrostatic stability to the GNPs [3, 4]. This process must be conducted carefully, as the drastic removal of the GNPs surfactant before functionalization of the biomolecules tends to reduce electrostatic stability and induce aggregation of the GNPs. Hence, the gradual removal of the surfactant is critical in the biomolecular functionalization of GNPs [5]. Conventionally, many researchers have employed a zeta potential analyzer to measure the

⁷ These authors contributed equally to this work.

⁸ Authors to whom any correspondence should be addressed.

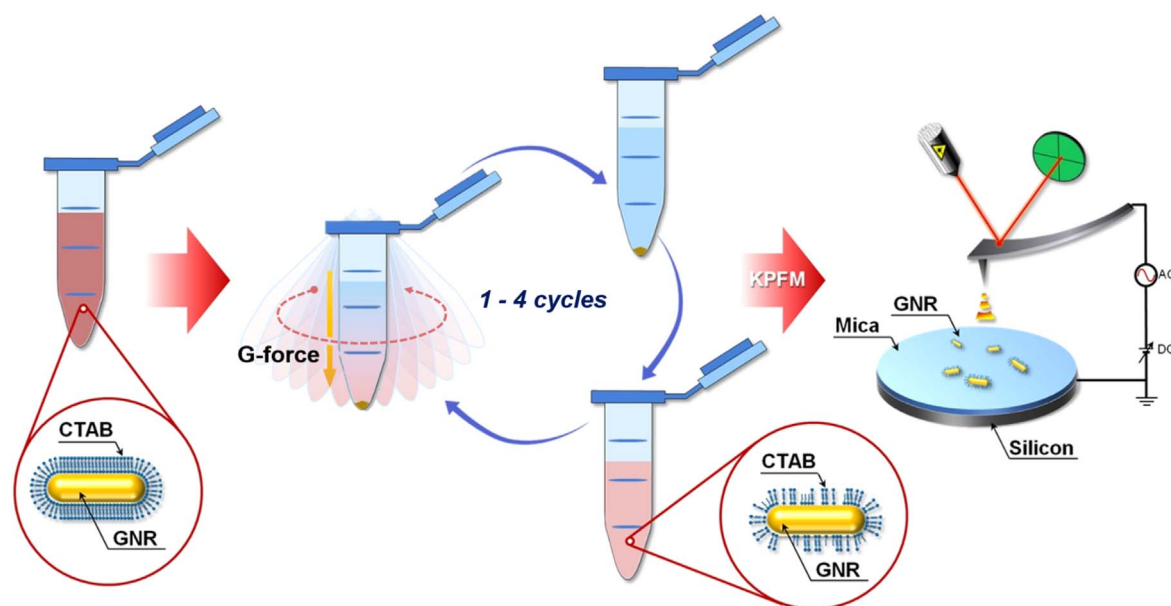


Figure 1. Schematic illustration of experimental process. Kelvin probe force microscopic (KPFM) analyses were conducted to measure surface potential of single gold nanorods (GNRs) in nanoscale range.

effectiveness of GNP surfactant removal. However, it is difficult for the zeta potential analysis to monitor the individual nanoelectrical properties of single GNPs during the surfactant removal process.

Recently, Kelvin probe force microscopy (KPFM) has been employed in the field of material science as a technique to provide worthwhile insights into the electronic properties of the sample surface, including the work function, conductivity, and surface dipoles [6–11]. Moreover, KPFM is a scanning probe microscopy (SPM) application technology, providing a quantitative differential measurement of the surface potential at the mV-scale with sufficient sensitivity for the detection of biomolecules and toxic materials [12–18]. KPFM is a highly effective technique for direct measurement of the contact potential differences between the conducting tip and the conducting surface [19]. It generally operates in two different modes (i.e. the lift mode and dual-frequency mode). Both modes have their advantages and disadvantages, while the lift mode is more suitable for the sensing of nanomaterials due to its relatively high signal-to-noise (S/N) ratio. In particular, a lift-mode KPFM has a dual-pass mechanism, where the topographic mapping is run on the first pass, and electrostatic surface potential mapping is run on the second pass, which follows the trajectory of the first mapping. In the second pass, the potential of the conducting tip applied for neutralization is used as signal output. Thus, KPFM provides the surface potential of samples independently from the topography of the sample. A lift-mode KPFM (i.e. the SPM technology with high S/N ratio) hence enables individual sensing of nanomaterials.

Herein, we report the direct measurement of the surfactant removal of the individual gold nanorods (GNRs) and gold nanospheres (GNSs) by using lift-mode KPFM (figure 1). We removed toxic capping agents (CTAB) by repeated centrifugation of the GNR solution. In the CTAB

removal process, we monitored the surface potential change of individual GNRs using KPFM. Further experiments with GNS were performed for another surfactant removal process (i.e. citrate) to observe the surface potential change of individual GNS using KPFM. In summary, the results indicate that KPFM-based techniques can provide more detailed information about the surfactant removal process compared to that provided by the zeta potential analysis. Our approach contributes to the investigation of the toxicity of metal NPs, depending on the amount of surfactants, and to the design of chemically modified NPs for biomedical applications.

Materials and methods

Synthesis of GNR

GNRs were synthesized by the seed-mediated method, [20] which uses CTAB as a surfactant at the surface of the GNRs. There was an excess of CTAB molecules at the surface of the GNRs. In brief, to prepare the gold-seed solution, 250 μl $\text{HAuCl}_4 \cdot 3\text{H}_2\text{O}$ (10 mM) solution was added to 7.5 ml of hexadecyltrimethylammonium bromide (CTAB) (93 mM) solution, and subsequently, 600 μl ice-cold sodium borohydride (10 mM) was added to the mixture by vigorous stirring. The mixture was allowed to react for 2 min, after which it was stored at room temperature (20 °C–25 °C) for 4 h. Then, a growth solution was prepared as follows. The CTAB solution was prepared under vigorous stirring, and 80 μl silver nitrate (10 mM) solution, 50 μl $\text{HAuCl}_4 \cdot 3\text{H}_2\text{O}$ (10 mM) solution, 55 μl ascorbic acid (100 mM) solution, and 12 μl gold-seed solution were successively added to the prepared CTAB solution and stirred for 30 s. The product solution was then stored at room temperature for 24 h.

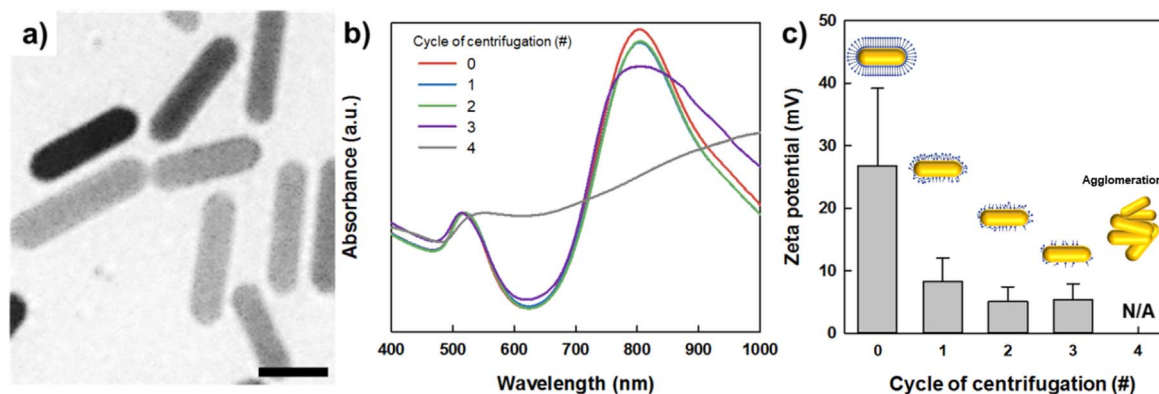


Figure 2. Characterization of GNR depending on number of centrifuge cycles. (a) Transmission electron microscope (TEM) image of GNRs. Scale bar represents 20 nm. (b) Absorbance spectra and (c) zeta potentials of GNRs according to number of centrifugation cycles.

Synthesis of GNS

All glassware was soaked in aqua regia (i.e. a mixture of nitric acid (HNO_3) and hydrochloric acid (HCl) at a ratio of 4:1) and rinsed with deionized (DI) water followed by Millipore water before use. AuNPs were synthesized by the citrate reduction method. [21, 22]. To prepare AuNPs with a 20 nm diameter, HAuCl_4 solution (1 mM, 100 ml) was heated at reflux while stirring. When the solution started to reflux, sodium citrate (38.8 mM, 10 ml) was added quickly. The solution was allowed to reflux for 30 min and then cooled naturally to room temperature (20°C – 25°C) under stirring.

Centrifugation of GNRs

The GNRs were separated from excess CTAB and then purified from the by-products by centrifugation. For this purpose, GNR (1 ml) sample was placed in a 2 ml centrifuge tube and kept at 20°C during centrifugation at 5000 rpm for 30 min to prevent crystallization of the CTAB. The supernatant was carefully removed with a pipette, leaving a volume of $\sim 50 \mu\text{l}$ along with the precipitate. The precipitates were resuspended by the addition of DI water (0.95 ml), resulting in a final volume of 1 ml.

Characterization of GNR

The morphological characterization of GNRs was carried out by transmission electron microscopy (TEM) using a JEM-1011 (JEOL, Japan) instrument. To characterize the optical properties, the UV–vis absorption spectra (400–1000 nm wavelength) of the GNRs were recorded by a spectrophotometer (PerkinElmer, USA) depending on the number of centrifuge cycles (0–4). Each spectrum was acquired with a scan rate of 600 nm s^{-1} . The zeta potential of the GNRs was measured using a particle analyzer (ELSZ-1000, Otsuka Electronics, Japan).

Tapping-mode AFM and KPFM analysis

To prepare samples for tapping-mode AFM and KPFM analysis, the GNR solution ($100 \mu\text{l}$), subjected to different numbers of centrifugation cycles (0–4), was dropped onto the

freshly cleaved surface of a p-type silicon substrate (Silicon Technology, Tokyo, Japan), and the GNR samples were adsorbed onto the substrate for 1 h. The substrate was then rinsed with deionized water and gently blow-dried with nitrogen to prevent the aggregation of GNRs before AFM imaging or surface potential measurements. The topography and surface potential measurements of all GNR cases were performed using a commercial AFM instrument (Multimode V, Veeco, CA, USA) at room temperature. A conducting cantilever tip (SCM-PIT, Bruker, CA, USA) exhibiting a resonance of $\sim 75 \text{ kHz}$ was mounted on a tip holder (MMEFCH, Veeco, USA) that enabled the control of the tip voltage. All KPFM images were produced with an image size of $10 \times 10 \mu\text{m}^2$ at a scanning rate of 0.5 Hz using lift-mode KPFM, which is appropriate for measuring small potential variations ($<100 \text{ mV}$) [23]. The lift-mode KPFM technique was employed because its properties are superior to those of the dual frequency-mode technique, resulting in precise imaging, higher resolution, and the prevention of sample damage and tip abrasion [14, 24]. We optimized the lift scan height (10 nm) and scan speed ($5 \mu\text{m s}^{-1}$) of the KPFM imaging based on our previous studies [14, 15], which demonstrated the functionality of nanoparticles/KPFM system and optimized the surface potential mapping conditions of nanoparticles using KPFM. Notably, tapping-mode AFM images were obtained simultaneously with surface potential mapping.

Principle of KPFM

KPFM measures the contact potential difference (V_{CPD}) between the conductive cantilever tip and the sample surface, which is defined as [25]:

$$V_{\text{CPD}} = \frac{\phi_{\text{tip}} - \phi_{\text{sample}}}{-e}, \quad (1)$$

where ϕ_{tip} and ϕ_{sample} are the work functions of the tip and the sample, respectively, and e is the electronic charge. KPFM obtains V_{CPD} by utilizing the electrostatic force (F_{es}) between

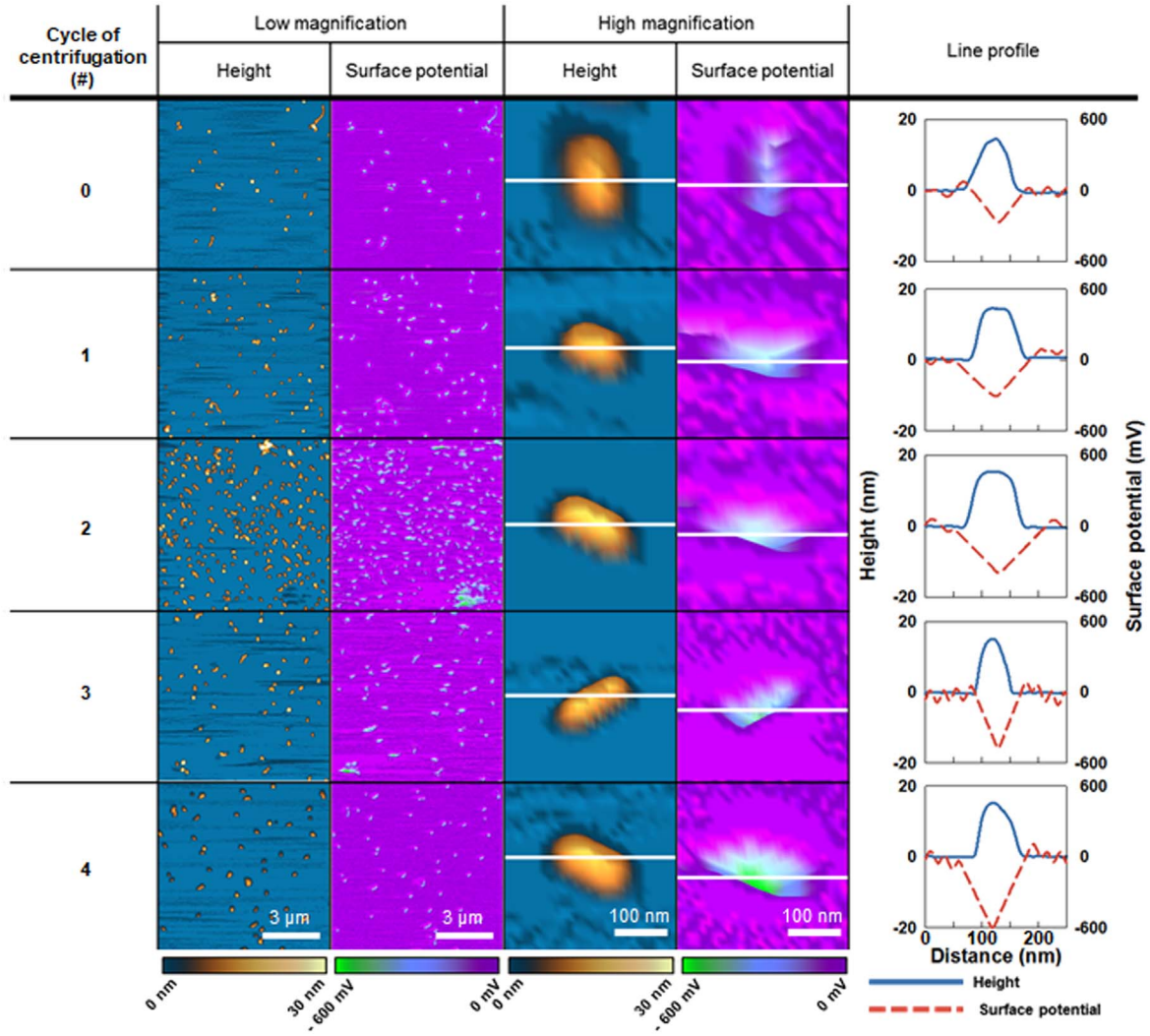


Figure 3. Height, surface potential map images, and corresponding cross-sectional profiles of GNRs according to number of centrifugation cycles.

the tip and the sample, which is given by [26]:

$$F_{es} = -\frac{1}{2}\Delta V^2 \frac{dC}{dz}, \quad (2)$$

where C is the capacitance, z is the distance between the AFM tip vertex and the sample surface, and ΔV is a voltage applied between the tip and the sample, given by:

$$\Delta V = (V_{DC} - V_{CPD}) + V_{AC} \sin \omega t, \quad (3)$$

where V_{DC} is the DC bias term of the applied voltage, and $V_{AC} \sin \omega t$ is the AC voltage term at the resonant frequency ω . In addition, substituting equation (3) for (2) yields a formula for F_{es} with the CPD term:

$$F_{es} = -\frac{dC}{dz} \left[\left\{ \frac{1}{2}(V_{DC} - V_{CPD}) \right\}^2 + (V_{DC} - V_{CPD})V_{AC} \sin \omega t + \frac{1}{4}V_{AC}^2 \{\cos(2\omega t) - 1\} \right]. \quad (4)$$

Applying the Kelvin probe method to equation (4), V_{CPD} is measured by applying V_{DC} to negate the ω component signal, such that F_{es} is zero. Consequently, the surface potential of the sample surface is mapped by adjusting the V_{DC} component.

Results and discussion

To demonstrate the utility of KPFM for the measurement of the surface potential of nanoparticles, GNRs were chosen as sample nanoparticles. Excess CTAB molecules (i.e. the surfactant on the surface of the GNRs) must be removed for biomedical applications, because they exhibit cytotoxicity and interfere with cellular functions due to their strong electrostatic potential [27, 28]. In the past, these CTAB molecules have been removed or reduced using centrifugation, however, to our knowledge, there have been no reports investigating the nanoscale-surface potential of nanoparticles by varying the concentration of the surfactant molecules at the nanoparticle surface by centrifugation.

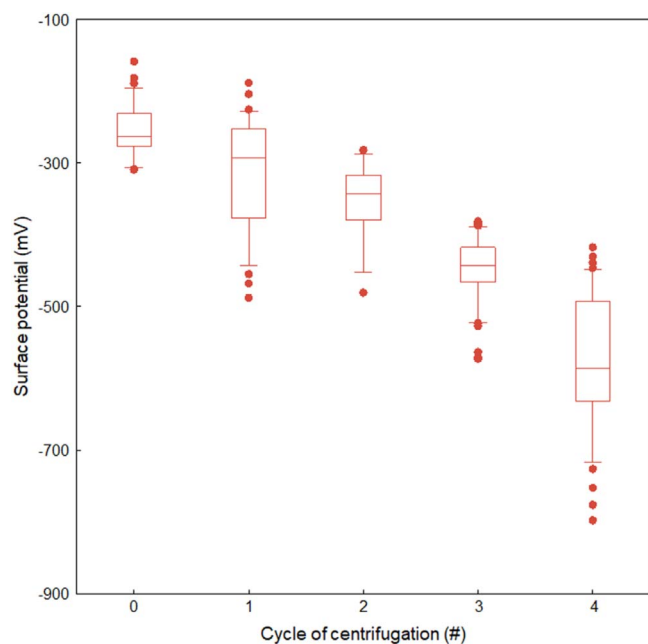


Figure 4. Box plot of surface potential distribution of GNRs with respect to number of centrifugation cycles (0–4).

Before the measurements of the GNR surface potential were recorded, the size and morphology of the GNRs were confirmed by TEM imaging (figure 2(a)), which showed that their aspect ratio (longitudinal length/transverse length) was 3.6 (36.0 ± 3.3 nm longitudinal length and 10.0 ± 1.1 nm transverse length). Without any centrifugation, the absorbance peaks of GNRs at 803 nm and 514 nm (UV-1800, Shimadzu, Japan) were observed, corresponding to the oscillations of electrons along the longitudinal and transverse axes of the GNR, respectively (figure 2(b)). Correlations between the aspect ratio and positions of the absorbance peaks were consistent with previously published research [29]. With the increasing number of cycles of centrifugation (from 0 to 3), the peak at 803 nm, corresponding to the longitudinal length of the GNRs, decreased slightly. Moreover, after four centrifugation cycles, the peak at 514 nm, corresponding to the transverse length of the GNRs, changed to shoulder-like shapes, and the peak at 803 nm disappeared. These results suggest that the GNRs aggregated because of the elimination of CTAB molecules, which acted as surfactants at the surface of the GNRs. In general, two forces stabilize nanoparticles: electrostatic and steric forces [30]. In the case of the GNRs, CTAB molecules, which have a strong electrostatic potential, provided electrostatic stabilization. The electrostatic interaction formed an electrical double layer around the GNRs with electrostatic repulsive forces. These repulsive forces can both stabilize and disperse GNRs in aqueous phase. With our experimental conditions, CTAB molecules were removed from the surface of the GNRs during the fourth centrifugation cycle. Accordingly, the electrostatic repulsion was eliminated, and the GNRs aggregated as a consequence.

The zeta potentials of the GNRs were likewise analyzed after each centrifugation cycle, because we hypothesized that the surface potentials of the GNRs could be inferred from

measurements of the zeta potentials (figure 2(c)). The zeta potentials were 26.8 ± 12.4 , 8.2 ± 3.8 , 5.1 ± 2.4 , and 5.4 ± 2.5 mV before centrifugation and after the first, second, and third centrifugation cycles, respectively. Results show that the CTAB molecules were gradually removed. Finally, the zeta potential was not measured after the fourth centrifugation cycle, which implied that the GNRs aggregated (figure 2(c)). This is because CTAB molecules were removed from the surface of GNRs, and the electrostatic repulsive force between the CTAB molecules became weaker than the van der Waals force [31]. The zeta potential can be defined as the potential difference between the dispersion medium and the stationary fluid layer attached to the dispersed particles [32]. Therefore, it is not equal to the surface potential, which is defined at different locations. Moreover, since only the ensemble average of the zeta potential of the GNRs is analyzed by the zeta analyzer, it is impossible to measure the individual GNR via zeta potential analysis [33]. Therefore, the change in surface potential of individual GNRs depending on the surfactant removal process remains unclear.

To investigate the surface potential of individual GNRs, we performed surface-potential mapping of the GNRs after each centrifugation cycle (0–4 centrifugation cycles). Figure 3 depicts the representative three-dimensional (3D) topography and surface-potential mapping of the GNRs obtained by KPFM after a different number of centrifugation cycles. All results were acquired at the optimal scan speed of $10 \mu\text{m s}^{-1}$ under ambient conditions. From the 3D topography mapping of the GNRs, we observed that the heights of the GNRs were almost identical, 15.00 ± 0.36 nm. However, the surface potential measurements of the GNRs revealed a consistent trend of surface potential distribution with respect to the number of centrifugation cycles, from 0 to 4. Specifically, the surface potential of the GNRs decreased from -264.56 to -601.61 mV as the number of centrifugation cycles increased (from 0 to 4), uncovering the negatively charged GNRs by removing the positively charged CTAB.

To precisely detect the surface potential of the GNRs, we further conducted quantitative and statistical analyses of the GNRs by constructing a box plot of the surface potential distribution on the GNRs according to the number of centrifugation cycles. The results show that from 20 to 100 individual complexes were captured in a single image for each condition (figure 4). The mean value for each condition was extracted from the analysis. Before any centrifugation cycles, the surface potential of GNR was -262.06 mV; after one centrifugation cycle, it was -292.92 mV, after two centrifugation cycles, it was -344.10 mV, after three cycles, it was -442.91 mV, and after four cycles, it was -585.79 mV. More specifically, as the number of centrifugation cycles increase, the charge of the GNRs decreases linearly, which represents that all of the CTAB molecules covering the surface of the GNR are not simultaneously removed. The results in figure 4 show that at least three centrifugation cycles are required to remove all CTAB molecules present on the surface of the GNR. In addition, at four cycles, the surface charge distribution of GNRs increases dramatically as a result

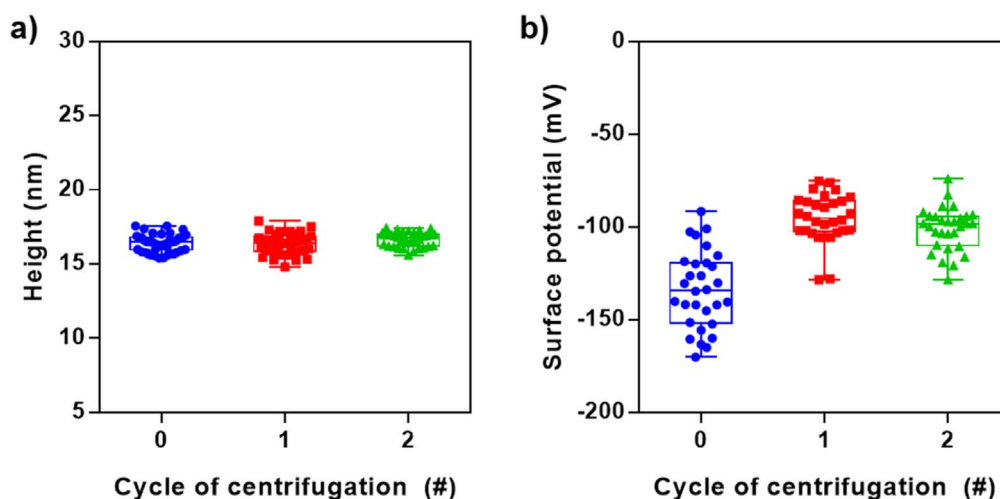


Figure 5. Box plot of (a) height and (b) surface potential distributions of gold nanospheres (20 nm) with respect to number of centrifugation cycles (0–4).

of the agglomeration of GNRs, which occurs due to the removal of all surfactant CTAB.

To investigate another type of NPs, we analyzed the surface potential of the GNS during the surfactant (citrate) removal process. Figure 5(a) shows the topographic measurements corresponding to the number of centrifugation cycles #0, #1, and #2 (16.5 ± 0.6 , 16.3 ± 0.7 , and 16.6 ± 0.5 nm, respectively). The results indicate that the average height of the GNS was not affected by 0–2 centrifugation cycles. In contrast, as shown in figure 5(b), the surface potential of each GNS (-133.8 ± 20.5 mV) was changed to -95.2 ± 12.6 mV after the first centrifugation cycle, suggesting that the capping agent (citrate) was detached from the GNS surface by centrifugation. These results were attributed to the fact that citrate (a trivalent anion) is more negative than is the bare surface of GNS [34, 35]. After two cycles of centrifugation, the surface potential of GNS was -100.9 ± 11.5 mV, similar to the surface potential after one cycles of centrifugation. The results indicated that citrate was mostly detached from the surface of GNPs, which implicated the low affinity between citrate and GNS [35, 36]. Overall, KPFM was capable of analyzing the nanoelectrical properties of GNSs and GNRs with respect to the removal of surfactants.

Conclusion

Nanoscale surface potentials of single gold nanoparticles were analyzed by a KPFM analytical method for up to four cumulative centrifugation cycles. The amount of the small molecule CTAB, acting as a surfactant on the GNR, was reduced by centrifugation, and the zeta potentials became indistinguishable with an increasing number of centrifugation cycles. In contrast, the surface potentials were successfully discriminated, even after four centrifugation cycles, which is the condition where GNRs aggregation was initiated. Moreover, we also observed that citrate removal process from GNS depended on the number of centrifugation cycles, and this phenomenon was observed through measurement of surface potential using the KPFM

analytical method. The surface potentials of GNS were different after only first centrifugation cycle due to the relatively low affinity between GNS and citrate. This study showed that KPFM-based techniques have the capability of characterizing the surfactant of individual nanoparticles with high-resolution by mapping the surface potential of single nanoparticles. This not only demonstrates a potential for the detection of small molecules, such as nucleic acids, ions, and drugs, but can also aid in designing engineered nanoparticles for biomedical applications.

Acknowledgments

This work was supported by the National Research Foundation of Korea (NRF) Grant funded by the Korean Government (MSIP) (No., NRF-2017R1A6A3A11034311, NRF-2018M3C1B7020722, and NRF-2019R1A2B5B01070617). Also, This work was supported by a grant of the Korea Health Technology R&D Project through the Korea Health Industry Development Institute (KHIDI), funded by the Ministry of Health & Welfare, Republic of Korea (HI16C0179 and HI17C2586).

ORCID iDs

Hyungbeen Lee <https://orcid.org/0000-0002-3218-5199>
 Dongtak Lee <https://orcid.org/0000-0001-8716-1736>
 Gyudo Lee <https://orcid.org/0000-0001-7895-5112>
 Jaemoon Yang <https://orcid.org/0000-0001-7365-0395>
 Dae Sung Yoon <https://orcid.org/0000-0002-6447-2862>

References

- [1] Dykman L and Khlebtsov N 2012 Gold nanoparticles in biomedical applications: recent advances and perspectives *Chem. Soc. Rev.* **41** 2256–82

- [2] Tiwari P M *et al* 2011 Functionalized gold nanoparticles and their biomedical applications *Nanomaterials* **1** 31–63
- [3] Lee D, Lee G and Yoon D S 2018 Anti-A β drug candidates in clinical trials and plasmonic nanoparticle-based drug-screen for Alzheimer's disease *Analyst* **143** 2204–12
- [4] Sato K, Hosokawa K and Maeda M 2003 Rapid aggregation of gold nanoparticles induced by non-cross-linking DNA hybridization *J. Am. Chem. Soc.* **125** 8102–3
- [5] Aldewachi H *et al* 2018 Gold nanoparticle-based colorimetric biosensors *Nanoscale* **10** 18–33
- [6] Cui X *et al* 2003 Controlling energy-level alignments at carbon nanotube/Au contacts *Nano Lett.* **3** 783–7
- [7] Lee G *et al* 2012 Mapping the surface charge distribution of amyloid fibril *Appl. Phys. Lett.* **101** 043703
- [8] Kwon T *et al* 2013 Carbon nanotube-patterned surface-based recognition of carcinoembryonic antigens in tumor cells for cancer diagnosis *J. Phys. Chem. Lett.* **4** 1126–30
- [9] Lee G *et al* 2015 Self-assembled amyloid fibrils with controllable conformational heterogeneity *Sci. Rep.* **5** 16220
- [10] Park J *et al* 2012 The work function of doped polyaniline nanoparticles observed by Kelvin probe force microscopy *Nanotechnology* **23** 365705
- [11] Gupta S, Loh K J and Pedtke A 2019 Sensing and actuation technologies for smart socket prostheses *Biomed. Eng. Lett.* (<https://doi.org/10.1007/s13534-019-00137-5>)
- [12] Park J *et al* 2011 Single-molecule recognition of biomolecular interaction via Kelvin probe force microscopy *ACS Nano* **5** 6981–90
- [13] Park J *et al* 2014 Ultra-sensitive direct detection of silver ions via Kelvin probe force microscopy *Biosens. Bioelectron.* **60** 299–304
- [14] Lee D *et al* 2018 Extremely sensitive and wide-range silver ion detection via assessing the integrated surface potential of a DNA-capped gold nanoparticle *Nanotechnology* **30** 085501
- [15] Kim W *et al* 2018 Al³⁺ ion sensing at attomole level via surface-potential mapping of gold nanoparticle complexes *Sensors Actuators B* **255** 2179–86
- [16] Lee H *et al* 2016 Kelvin probe force microscopy of DNA-capped nanoparticles for single-nucleotide polymorphism detection *Nanoscale* **8** 13537–44
- [17] Lee H *et al* 2018 Identifying DNA mismatches at single-nucleotide resolution by probing individual surface potentials of DNA-capped nanoparticles *Nanoscale* **10** 538–47
- [18] Glatzel T *et al* 2002 CuGaSe₂ solar cell cross section studied by Kelvin probe force microscopy in ultrahigh vacuum *Appl. Phys. Lett.* **81** 2017–9
- [19] Barth C *et al* 2011 Recent trends in surface characterization and chemistry with high-resolution scanning force methods *Adv. Mater.* **23** 477–501
- [20] Hong Y *et al* 2013 Localized surface plasmon resonance based nanobiosensor for biomarker detection of invasive cancer cells *J. Biomed. Opt.* **19** 051202
- [21] Kimling J *et al* 2006 Turkevich method for gold nanoparticle synthesis revisited *J. Phys. Chem. B* **110** 15700–7
- [22] Liu J and Lu Y 2006 Preparation of aptamer-linked gold nanoparticle purple aggregates for colorimetric sensing of analytes *Nat. Protocols* **1** 246
- [23] Sinensky A K and Belcher A M 2007 Label-free and high-resolution protein/DNA nanoarray analysis using Kelvin probe force microscopy *Nat. Nanotechnol.* **2** 653
- [24] Druker B J and Lydon N B 2000 Lessons learned from the development of an abl tyrosine kinase inhibitor for chronic myelogenous leukemia *J. Clin. Invest.* **105** 3–7
- [25] Nonnenmacher M, O'Boyle M and Wickramasinghe H K 1991 Kelvin probe force microscopy *Appl. Phys. Lett.* **58** 2921–3
- [26] Melitz W *et al* 2011 Kelvin probe force microscopy and its application *Surf. Sci. Rep.* **66** 1–27
- [27] Alkilany A M *et al* 2009 Cellular uptake and cytotoxicity of gold nanorods: molecular origin of cytotoxicity and surface effects *Small* **5** 701–8
- [28] Hong Y *et al* 2012 Gold nanorod-mediated photothermal modulation for localized ablation of cancer cells *J. Nanomater.* **2012** 2
- [29] Link S, Mohamed M B and El-Sayed M A 1999 Simulation of the optical absorption spectra of gold nanorods as a function of their aspect ratio and the effect of the medium dielectric constant *J. Phys. Chem. B* **103** 3073–7
- [30] Aragay G, Pons J and Merkoçi A 2011 Recent trends in macro-, micro-, and nanomaterial-based tools and strategies for heavy-metal detection *Chem. Rev.* **111** 3433–58
- [31] Kim T *et al* 2008 Kinetics of gold nanoparticle aggregation: experiments and modeling *J. Colloid Interface Sci.* **318** 238–43
- [32] Clogston J D and Patri A K 2011 Zeta potential measurement *Characterization of Nanoparticles Intended for Drug Delivery*. (Berlin: Springer) pp 63–70
- [33] Honary S and Zahir F 2013 Effect of zeta potential on the properties of nano-drug delivery systems-a review (Part 1) *Tropical J. Pharm. Res.* **12** 255–64
- [34] Zhao P, Li N and Astruc D 2013 State of the art in gold nanoparticle synthesis *Coord. Chem. Rev.* **257** 638–65
- [35] Park J-W and Shumaker-Parry J S 2014 Structural study of citrate layers on gold nanoparticles: role of intermolecular interactions in stabilizing nanoparticles *J. Am. Chem. Soc.* **136** 1907–21
- [36] Wang S *et al* 2012 Comparison of the peroxidase-like activity of unmodified, amino-modified, and citrate-capped gold nanoparticles *Chem. Phys. Chem* **13** 1199–204